

Collisional-radiative average-atom model for hot plasmas

Balazs F. Rozsnyai

Lawrence Livermore National Laboratory, P.O. Box 808, Livermore, California 94551

(Received 17 December 1996)

A collisional-radiative “average-atom” (AA) model is presented for the calculation of opacities of hot plasmas that are not in the condition of local thermodynamic equilibrium (LTE). The electron impact and radiative rate constants are calculated using the dipole oscillator strengths of the average atom. A key element of the model is the photon escape probability, which at present is calculated for a semi-infinite slab. The Fermi statistics renders the rate equations for the AA level occupancies nonlinear, which requires iterations until the steady-state AA level occupancies are found. Detailed electronic configurations are built into the model after the self-consistent non-LTE AA state is found. The model shows a continuous transition from the non-LTE to the LTE state depending on the optical thickness of the plasma. [S1063-651X(97)03406-5]

PACS number(s): 52.25.-b

I. INTRODUCTION

Models for calculating equation of state (EOS) data and photoabsorption cross sections of hot plasmas in the state of local thermodynamic equilibrium (LTE) have been around for some time [1–9]. Under LTE conditions the Fermi and Boltzmann statistics define the distribution of the quantum mechanical states of the radiating ions and of the free electrons around them, thus greatly facilitating the theoretical development of the model. The condition of LTE is assured when the plasma is completely dominated by collisions and/or when the radiation field surrounding the plasma is Planckian. In the absence of the above the statistical distribution of the different ionic states can be obtained only by solving the relevant rate equations involving the ions and photons. Previous papers addressing the subject of ionization balance in terms of the steady-state solutions of the rate equations used either semiclassical and parametrized atomic data [10], or the hydrogenic approximation or isolated atomic data for the rate constants [11–15]. The problem of obtaining a set of rate equations for medium- or high- Z elements in dense plasmas is complicated by a number of factors. First, the number of quantum states of the different many-electron configurations can be enormous. Second, even when data of these quantum states are available for isolated atoms and ions, the plasma electrons may sufficiently perturb those states to the degree that they may be useless. Third, the non-LTE photon distribution has to be coupled self-consistently to the statistical distribution of the many-electron ionic states. To overcome the first and second difficulties we propose a set of rate equations using the average-atom (AA) approach, which treats the plasma by one representative “average atom,” which subsequently can be augmented with the details of the physically significant many-electron configurations. We will address the third problem with some limitations, as will be clearer below. The AA model under LTE conditions is described in Refs. [4–6] and in references given there. The AA approach to the rate equations is complicated by the fact that the Fermi statistics renders the rate equations nonlinear in terms of the AA level populations. For this reason at present we restrict our considerations to the steady-state solution of the rate equations

and will not consider time-dependent problems. For the present we restrict ourselves to the case when the photon distribution is derived from a Planckian field where the energy-dependent photon density is reduced by the probability of photon escape. This photon escape probability is coupled self-consistently to the quantum states of the AA atom. In Sec. II we present the basics of the model and in Sec. III we present computational results.

II. DESCRIPTION OF THE MODEL

A. Rate constants

In this subsection we consider the rate constants that enter the rate equations. We consider excitations, deexcitations, and ionizations by electron and photon impact. We assume that the electron thermalization time is short enough to assume a Maxwellian (or Fermi-Dirac) distribution for the free electrons, thus an electron temperature for the free states is well defined. Also we restrict ourselves to dipole-allowed transitions. The cross sections that determine the rate constants are approximations of precise quantum-mechanical calculations and were used before to calculate electron impact widths [16]. We start with the excitation cross section from a bound AA level i to another j by electron impact:

$$\sigma_{ij}^c(x) = 1.2\pi a_0^2 \left(\frac{e^2}{a_0}\right) \frac{f_{ij}}{(\Delta E_{ij})^2} [1 - \exp(-0.3x)] \frac{\ln x}{x}, \quad (2.1)$$

where ΔE_{ij} is the excitation energy, f_{ij} is the dipole oscillator strength normalized to one electron occupancy of the initial state i and computed from the AA wave functions, $x = \varepsilon/\Delta E_{ij}$ with ε as the energy of the incident electron, and the superscript c indicates “collision.” Equation (2.1) was obtained by a series of numerical fits to R -matrix calculations for dipole-allowed transitions in medium- Z atoms and ions. The general expression for the excitation rate is given by

$$R_{ij}^c = \int_{\Delta E_{ij}}^{\infty} \sigma_{ij}^c(\varepsilon) v(\varepsilon) n(\varepsilon) d\varepsilon \quad (\text{sec}^{-1}), \quad (2.2)$$

where v stands for the velocity. In the case of a Maxwellian distribution, the number of free electrons between ε and $\varepsilon + d\varepsilon$ is given by

$$\begin{aligned} n(\varepsilon)d\varepsilon &= \frac{2}{\sqrt{\pi}} \rho \frac{1}{(kT)^{3/2}} \varepsilon^{1/2} \exp(-\varepsilon/kT) d\varepsilon \\ &= \frac{2}{\sqrt{\pi}} \rho \frac{1}{(kT)^{3/2}} (\Delta E_{ij})^{3/2} x^{1/2} \\ &\quad \times \exp(-x\Delta E_{ij}/kT) dx, \end{aligned} \quad (2.3)$$

where kT stands for the temperature (in energy units) of the free electron gas with k denoting Boltzmann's constant and ρ for the total free electron density. Using $v = c(2\varepsilon/mc^2)^{1/2}$ we obtain

$$\begin{aligned} R_{ij}^c &= 1.2 \left(\frac{8\pi}{mc^2} \right)^{1/2} \frac{f_{ij}}{(kT)^{3/2}} e^4 c \rho \int_1^\infty [1 - \exp(-0.3x)] \ln x \\ &\quad \times \exp(-x\Delta E_{ij}/kT) dx \\ &= f_{ij} I_{ij}^{\text{ex}} (\text{sec}^{-1}), \end{aligned} \quad (2.4)$$

where we factored out the dipole oscillator strength. The integral in Eq. (2.4) is given by

$$\frac{kT}{\Delta E_{ij}} E_1 \left(\frac{\Delta E_{ij}}{kT} \right) - \frac{kT}{\Delta E_{ij} + 0.3kT} E_1 \left(\frac{\Delta E_{ij} + 0.3kT}{kT} \right), \quad (2.5)$$

where E_1 stands for the exponential integral. For the deexcitation (supereleastic) rates we have

$$R_{ji}^c = \frac{f_{ji}}{f_{ij}} \exp(\Delta E_{ij}/kT) R_{ij}^c \rightarrow (\text{detailed balance}). \quad (2.6)$$

The last relation is due to the fact that the deexcitation cross section is the same as Eq. (2.1) except the $\ln(x)$ term has to be replaced by $\ln(x+1)$. We calculate the electron impact ionization rates from the cross section

$$\sigma_{ic}^c(x) = \frac{K}{\varepsilon_i^2} e^4 [1 - 0.3 \exp(x)] \frac{\ln x}{x}, \quad x = \frac{\varepsilon}{|\varepsilon_i|}, \quad (2.7)$$

where ε and ε_i stand for the energy of the incident electron and for the eigenenergy of the bound level i , respectively, and the subscript c indicates the transition to a continuum state. Equation (2.7) is analogous to Eq. (2.1) and, apart from the exponential term, to Lotz's cross section for electron impact ionization [17]. For the best fit to agree with more sophisticated calculations we use $K = 2.27$. The ionization rate constant is given by

$$\begin{aligned} R_{ic}^c &= K e^4 \frac{2^{3/2}}{(\pi m c^2)^{1/2}} \frac{c \rho}{(kT)^{3/2}} \int_1^\infty [1 - \exp(-0.3x)] \ln x \exp \\ &\quad \times (-x|\varepsilon_i|/kT) dx (\text{sec}^{-1}). \end{aligned} \quad (2.8)$$

The condition of detailed balance relates the three-body recombination to Eq. (2.8) by

$$R_{ci}^c = \exp[(\mu - \varepsilon_i)/kT] R_{ic}^c, \quad (2.9)$$

where μ is the Fermi level of the free electron gas. Since $\exp(\mu/kT)$ is proportional to ρ and so is R_{ic}^c , Eq. (2.9) indeed represents three-body recombination. The condition $N_i R_{ic}^c = (g_i - N_i) R_{ci}^c$ leads to the Fermi statistics where N_i stands for the population of level i and g_i for its statistical weight. We account for the dielectronic recombination and its inverse by the Auger matrix elements A_{ji}^{mc} , which stands for an Auger process where an electron from level m goes to continuum while an other from level j fills a lower hole state in i . In the AA approximation this matrix element is given by [18]

$$A_{ji}^{mc} = \frac{2\pi}{\hbar} N_j N_m \sum_{l_c} (2l_i + 1)(2l_c + 1) a_i a_c (B_1 + B_2 + B_{12}), \quad (2.10a)$$

where

$$\begin{aligned} B_1 &= \sum_k \frac{1}{2k+1} \begin{pmatrix} l_j & k & l_i \\ 0 & 0 & 0 \end{pmatrix}^2 \begin{pmatrix} l_m & k & l_c \\ 0 & 0 & 0 \end{pmatrix}^2 \\ &\quad \times [R^k(n_j l_j n_m l_m; n_i l_i c l_c)]^2, \end{aligned} \quad (2.10b)$$

$$\begin{aligned} B_2 &= \sum_p \frac{1}{2p+1} \begin{pmatrix} l_m & p & l_i \\ 0 & 0 & 0 \end{pmatrix}^2 \begin{pmatrix} l_j & p & l_c \\ 0 & 0 & 0 \end{pmatrix}^2 \\ &\quad \times [R^p(n_m l_m n_j l_j; n_i l_i c l_c)]^2, \end{aligned} \quad (2.10c)$$

$$\begin{aligned} B_{12} &= (-1)^\lambda \sum_k \frac{1}{2k+1} \begin{pmatrix} l_j & k & l_i \\ 0 & 0 & 0 \end{pmatrix} \begin{pmatrix} l_m & k & l_c \\ 0 & 0 & 0 \end{pmatrix} \\ &\quad \times \sum_p \frac{1}{2p+1} \begin{pmatrix} l_m & p & l_i \\ 0 & 0 & 0 \end{pmatrix} \begin{pmatrix} l_j & p & l_c \\ 0 & 0 & 0 \end{pmatrix} \\ &\quad \times \begin{Bmatrix} l_m & l_c & k \\ l_j & l_i & p \end{Bmatrix} R^k(n_j l_j n_m l_m; n_i l_i c l_c) \\ &\quad \times R^p(n_m l_m n_j l_j; n_i l_i c l_c), \end{aligned} \quad (2.10d)$$

where $\lambda = l_j + l_i + l_m + l_c + 1$ and R stands for the usual Slater integrals. Also, in Eq. (2.10a) a stands for the availability of the states i and c given by

$$a_i = 1 - \frac{N_i}{g_i} \quad (2.10e)$$

for a bound state and

$$a_c = \frac{\exp[(\varepsilon_c - \mu)/kT]}{\exp[(\varepsilon_c - \mu)/kT] + 1} \quad (2.10f)$$

for a continuum state.

The symbols n and l stand for the principal and angular momentum quantum numbers, respectively. It should be noted that Eqs. (2.10a)–(2.10d) have nothing to do with the thermal state of the plasma. They are strictly the results of taking the Auger matrix elements between averaged J states.

In the case of photoabsorption we consider the photon escape probability due to the finite optical thickness. The concept of photon escape probability was used in previous works in connection with line transfers [19–21]. In this work we calculate the photon escape probability from the total self-consistent photoabsorption cross section, which includes the line profiles together with photoionization and inverse bremsstrahlung. We assume that the radiating ion is situated in a semi-infinite slab at a distance d away from the edge of the slab. For this case it is easy to show that the photon escape probability is given by

$$P(\hbar\omega) = \exp(-x) - xE_1(x), \quad (2.11)$$

where $x = d/l$; $l = 1/\sigma(\hbar\omega)D$, with σ and D the photoabsorption cross section and ion density of the plasma. Actually, we will use the photon confinement probability P_c , which is $1 - P$. Next, we consider the radiative transitions. For a spontaneous downward transition we have Einstein's transition probability

$$A_{ji} = \frac{2\alpha}{\hbar} \frac{(\Delta E_{ij})^2}{mc^2} f_{ji} \quad (\text{sec}^{-1}). \quad (2.12)$$

For an induced transition we use the general form

$$B_{ij} = c \int \sigma_{ij}(\hbar\omega) N(\hbar\omega) d(\hbar\omega) \quad (\text{sec}^{-1}), \quad (2.13)$$

where $N(\hbar\omega)d(\hbar\omega)$ is the number of photons/cm³ in the energy interval $\hbar\omega$ and $\hbar\omega + d(\hbar\omega)$. For the absorption cross section we have

$$\sigma_{ij}(\hbar\omega) = \frac{2\pi^2 e^2}{mc} \hbar f_{ij} b_{ij}(\hbar\omega) \quad (\text{cm}^2), \quad (2.14)$$

where $b_{ij}(\hbar\omega)$ is the line-shape function of the transition. Assuming a Dirac δ function for the line shape we have

$$B_{ij} = \frac{2\pi^2 e^2}{m} \hbar f_{ij} N(\hbar\omega_{ij}). \quad (2.15)$$

For a Planckian radiation field we have

$$N_P(\hbar\omega) = \frac{\omega^2}{\hbar\pi^2 c^3} \frac{1}{\exp(\hbar\omega/kT) - 1}. \quad (2.16)$$

We mimic the finite optical thickness with a photon distribution $N(\hbar\omega) = N_P(\hbar\omega)P_c(\hbar\omega)$ and obtain

$$B_{ij} = \frac{2\alpha}{\hbar} \frac{(\hbar\omega_{ij})^2}{mc^2} f_{ij} \frac{1}{\exp(\hbar\omega_{ij}/kT) - 1} P_c(\hbar\omega_{ij}). \quad (2.17)$$

For the downward j - i transition the combined spontaneous and induced rates give

$$A_{ji} + B_{ji} = \frac{2\alpha}{\hbar} \frac{(\Delta E_{ij})^2}{mc^2} f_{ji} \left[1 + \frac{1}{\exp(\hbar\omega_{ij}/kT) - 1} P_c(\hbar\omega_{ij}) \right]. \quad (2.18)$$

For the photoionization rate from a bound state m to the continuum c we use a lower case notation when P_c is less than 1,

$$r_{mc}^r = \frac{8\pi}{h^3 c^2} \int_{|\varepsilon_m|}^{\infty} (\hbar\omega)^2 \sigma_{m,c}(\hbar\omega) P_c(\hbar\omega) \times \exp(-\hbar\omega) d(\hbar\omega) \quad (\text{sec}^{-1}), \quad (2.19)$$

where P_c stands for the frequency-dependent photon confinement factor and $\sigma_{m,c}$ is the photoionization cross section of the level m normalized to one electron occupancy. It should be noted that Eq. (2.19) includes the induced downward $c \rightarrow m$ transition. The inverse radiative recombination is given by

$$R_{cm}^r = \exp[(\mu - \varepsilon_m)/kT] R_{mc}^r, \quad (2.20)$$

where R_{mc}^r refers to the photoionization rate in the optically thick case and is given by the same integral as Eq. (2.19) with $P_c = 1$. Equation (2.20) reflects the principle of detailed balance when the free electrons follow the Fermi statistics. It should be emphasized that the difference between the quantities of R_{mc}^r , which refers to a Planckian radiation field, and r_{mc}^r , which is the photoionization rate constant for the optically thin case, is crucial for determining the difference between the LTE and non-LTE level populations.

B. Rate equations

First, we summarize the rate constants that drive the rate equations: R_{mk}^c is the excitation (deexcitation) rate constant from level m to level k by electron impact. For radiative transitions between bound states we use

$$R_{mk}^r = B_{mk}$$

[in Eq. (2.17)] for upward transitions and

$$R_{mk}^r = A_{mk} + B_{mk}$$

[in Eq. (2.18)] for downward transitions.

R_{mc}^c is the rate constant for electron impact ionization from level m to continuum. The reverse, three body recombination rate constant is

$$R_{cm}^c = \exp[(\mu - \varepsilon_m)/kT] R_{mc}^c. \quad (2.21)$$

r_{mc}^r is the rate constant for photoionization for optically thin case. The reverse, radiative recombination rate constant is

$$R_{cm}^r = \exp[(\mu - \varepsilon_m)/kT] R_{mc}^r. \quad (2.22)$$

A_{ji}^{mc} is the rate constant for the Auger process in which an electron from level m goes to continuum while an other from level j fills a hole state in i , and A_{ij}^{cm} is the inverse. N_c is the number of free electrons per AA.

The availability of the state k is

$$a_k = 1 - N_k/g_k.$$

All rate constants are normalized to one-electron occupancies of the bound levels and they do not include the availability of the final state. Assuming that the number of bound AA levels is finite the rate equations are given by

$$\begin{aligned}
\frac{dN_m}{dt} = & - \underbrace{\left[\sum_{k=1}^b (R_{mk}^c N_c + R_{mk}^r) a_k \right]}_1 N_m - \underbrace{(R_{mc}^c N_c + r_{mc}^r)}_2 N_m - \underbrace{\left(\sum_j \sum_i N_j (g_i - N_i) A_{ji}^{mc} \right)}_3 N_m + \underbrace{\left[\sum_{k=1}^b (R_{km}^c N_c + R_{km}^r) N_k \right]}_4 a_m \\
& + \underbrace{(R_{cm}^c N_c + R_{cm}^r)}_5 (g_m - N_m) + \underbrace{\left(\sum_j \sum_i (g_j - N_j) N_i A_{ij}^{cm} \right)}_6 (g_m - N_m),
\end{aligned} \tag{2.23}$$

$$\begin{aligned}
\frac{dN_c}{dt} = & \underbrace{\sum_m (R_{mc}^c N_c + r_{mc}^r)}_7 N_m - \underbrace{\sum_m (R_{cm}^c N_c + R_{cm}^r)}_8 (g_m - N_m) + \underbrace{\sum_m \sum_j \sum_i \left[N_j N_m (g_i - N_i) A_{ji}^{mc} - N_i (g_m - N_m) (g_j - N_j) A_{ij}^{cm} \right]}_9 \underbrace{}_{10}.
\end{aligned} \tag{2.24}$$

All summations go over the bound level indices. It is easy to see that Eqs. (2.23) and (2.24) satisfy the particle conservation

$$\sum_j \sum_i N_j (g_i - N_i) A_{ji}^{mc} = K_{mc} \tag{2.25a}$$

and

$$\sum_m \frac{dN_m}{dt} + \frac{dN_c}{dt} = 0 \tag{2.25b}$$

$$\sum_j \sum_i N_i (g_j - N_j) A_{ij}^{cm} = \exp[(\mu - \varepsilon_m)/kT] K_{cm}.$$

because the sums with respect to m in terms 1 and 4 cancel out, the sum of term 2 with respect to m cancels out term 7, the same for terms 3 and 8, 5 and 9, and 6 and 10. The above is simply the consequence of particle number conservation. In a steady-state solution we must have $dN_c/dt=0$ separately, which means that the sums 7, 8, 9, and 10 have to add up to zero. This last condition defines the steady-state ionization balance, LTE or not. Next, we introduce some new quantities from the triple sums 9 and 10.

Let

Using the relationships (2.21) and (2.22) for the detailed balance and then Eq. (2.24) for the steady-state case one has the general form

$$\begin{aligned}
\frac{dN_c}{dt} = & \sum_m \{ (R_{mc}^c N_c + r_{mc}^r + K_{mc}) N_m - \exp[(\mu - \varepsilon_m)/kT] \\
& \times (g_m - N_m) (R_{m,c}^c N_c + R_{m,c}^r + K_{cm}) \} \\
= & 0.
\end{aligned} \tag{2.26}$$

TABLE I. Equivalent LTE temperatures, ionization states, and Fermi levels.

x_R	kT_{eq} (keV)	N_c	$-\mu/kT$	$-\mu_{\text{eq}}/kT_{\text{eq}}$
Pr($Z=59$) at $kT=1$ keV and 0.1 g/cm ³ $L_R=1.3619$ cm				
0.0000	0.20313	28.81	9.6756	7.3283
0.0001	0.44531	40.93	9.3293	8.1022
0.01	0.84375	49.01	9.1515	8.9023
1.0	1.0	50.70	9.1178	9.1178
LTE	1.0	50.77	9.1178	
Ge($Z=32$) at $kT=500$ eV 0.01 g/cm ³ $L_R=46.87$ cm				
0.0000	0.11523	19.357	10.669	8.4899
0.0001	0.15234	21.924	10.546	8.8217
0.01	0.42188	29.126	10.265	10.007
LTE	0.5	29.745	10.244	
LASNEX		23.377	10.482	

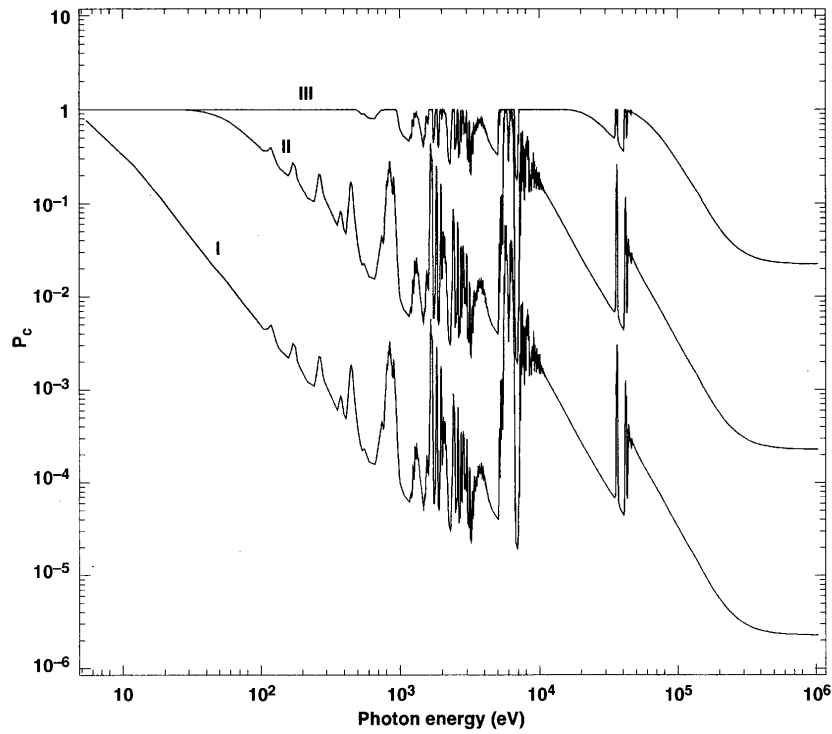


FIG. 1. Photon confinement factors of praseodymium vs photon energy at $kT=1$ keV, 0.1 g/cm^3 density with $x_R=10^{-4}$ (I), 10^{-2} (II), and $x_R=1$ (III).

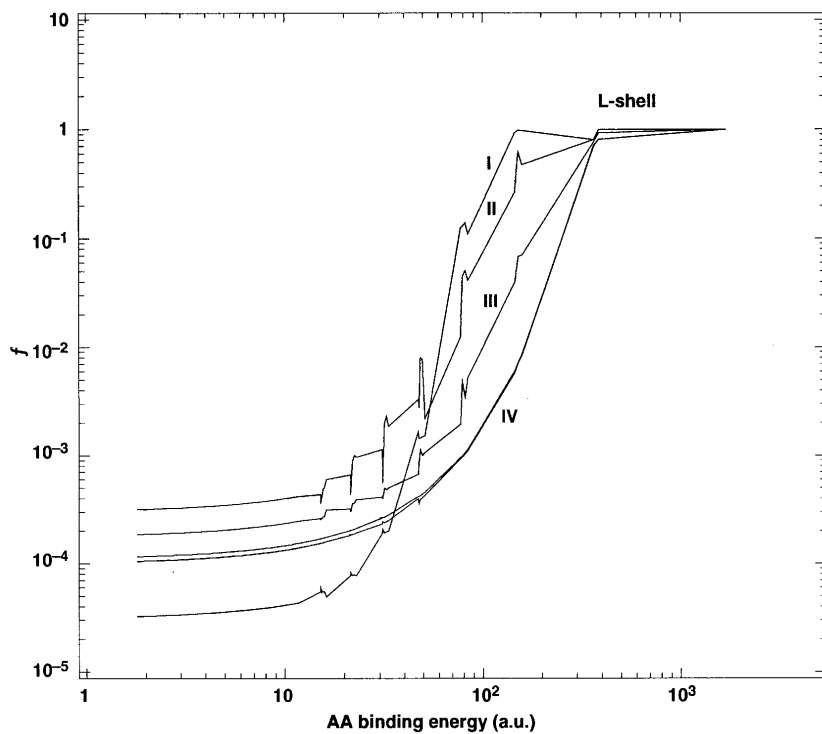


FIG. 2. Fermi functions of praseodymium at $kT=1$ keV and at 0.1 g/cm^3 density. The curves marked (I), (II), (III), and (IV) correspond to $x_R=0$, 10^{-4} , 10^{-2} , and 1 together with the LTE case, respectively.

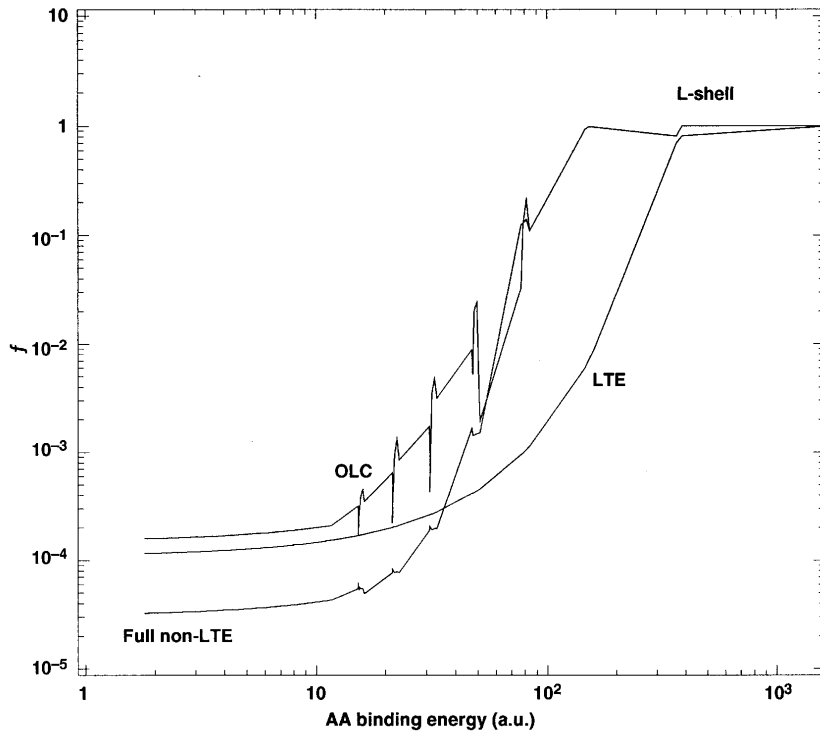


FIG. 3. Comparison of the OLC and full non-LTE Fermi functions with the LTE case of praseodymium at $kT=1$ keV and at 0.1 g/cm³ density with $x_R=0$.

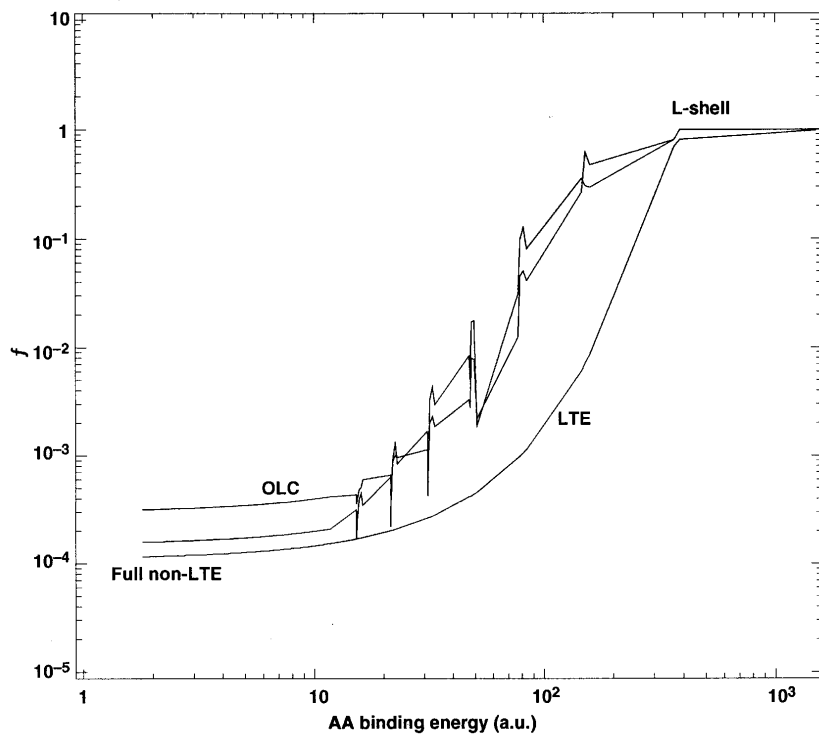


FIG. 4. Same as Fig. 3 with $x_R=10^{-4}$.

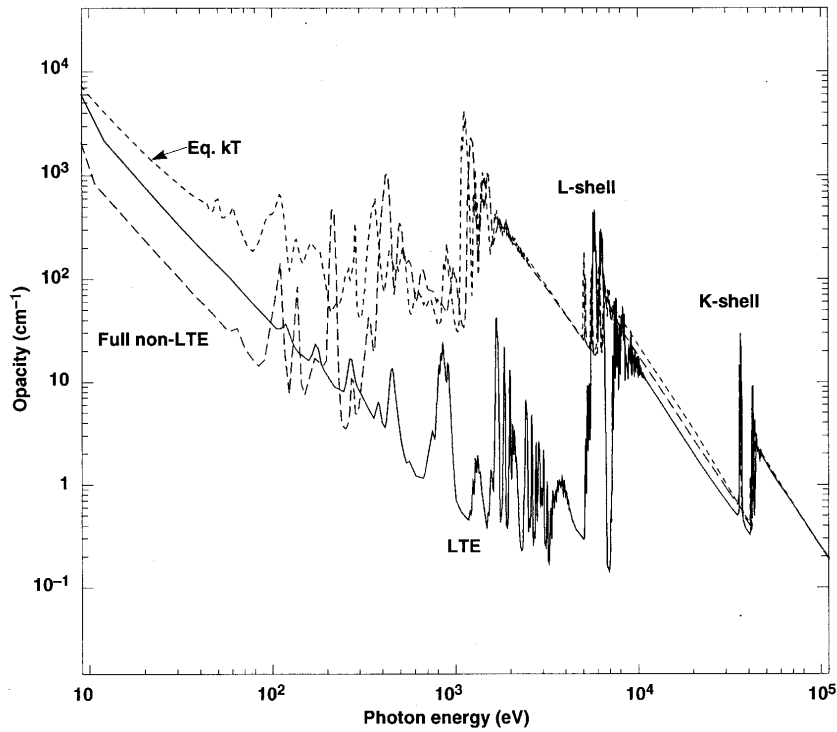


FIG. 5. Calculated opacities in cm^{-1} of praseodymium at $kT=1$ keV and at 0.1 g/cm^3 density with $x_R=0$. Full curve: LTE; long-dashed curve: full non-LTE based on the rate equations; short-dashed curve: LTE with the equivalent LTE temperature of 0.20313 keV from Table I.

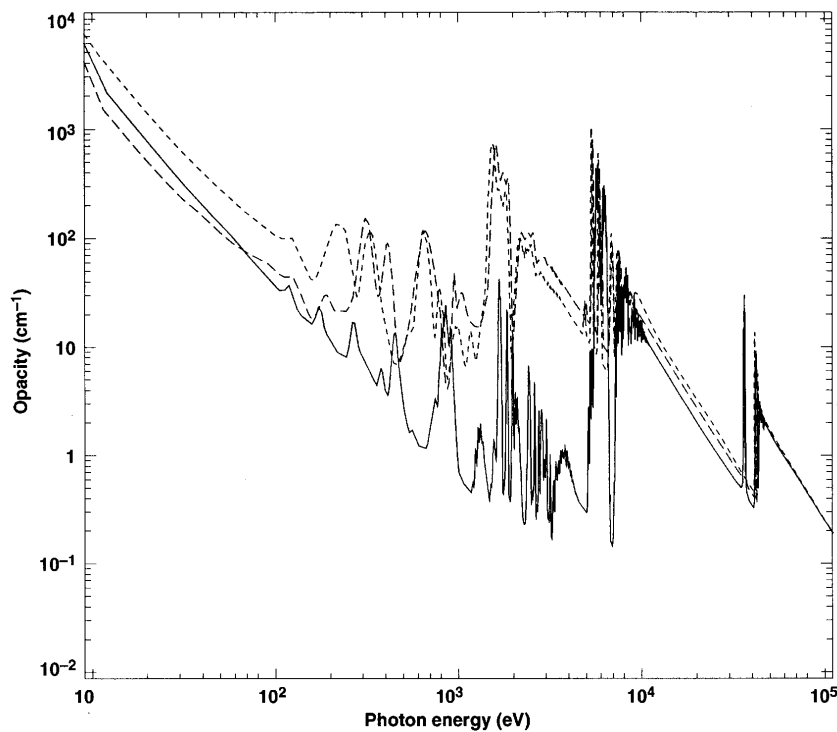


FIG. 6. Same as Fig. 5 with $x_R=10^{-4}$.

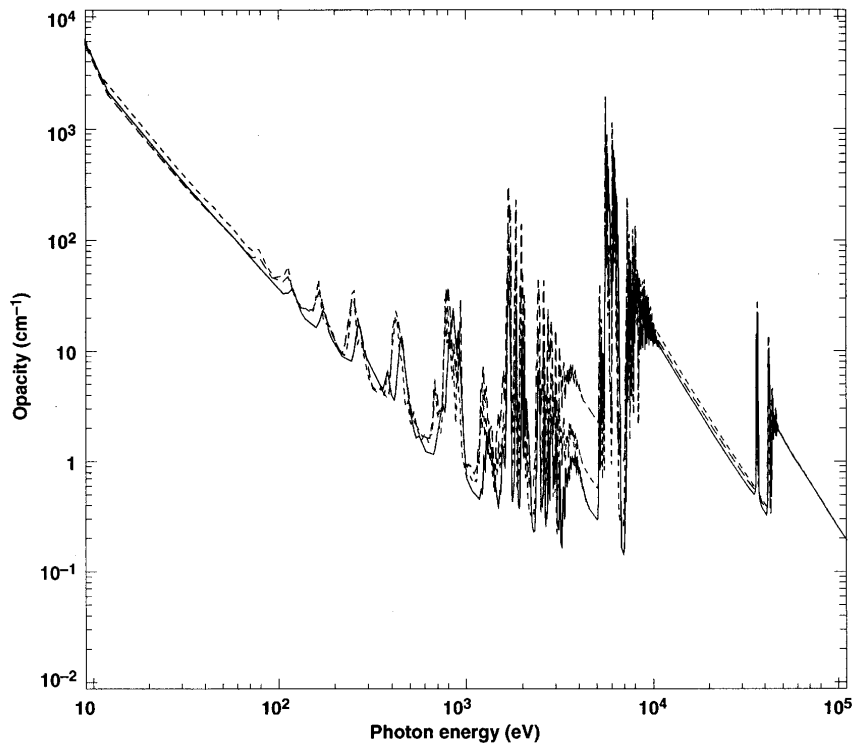


FIG. 7. Same as Fig. 5 with $x_R = 10^{-2}$.

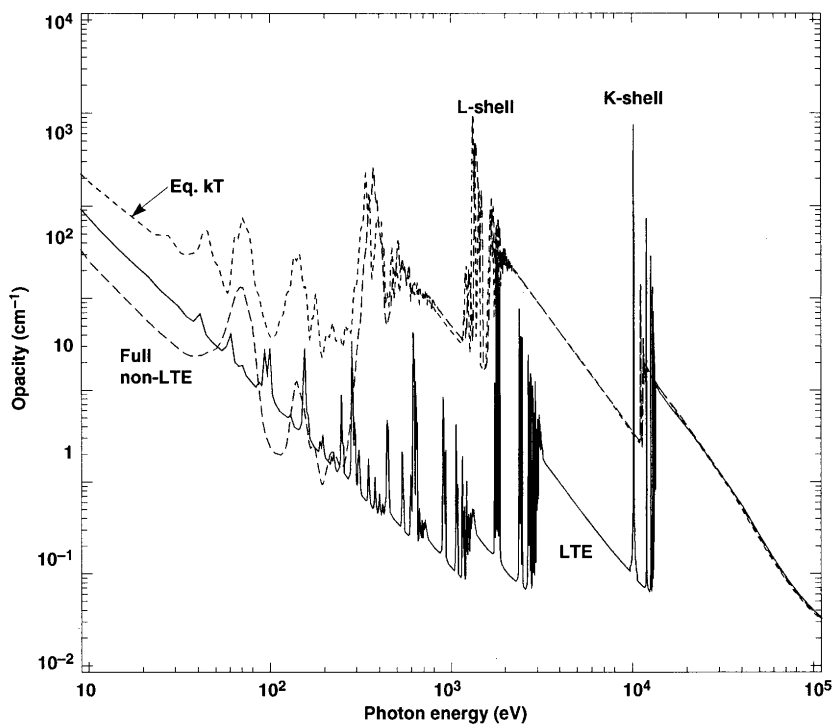
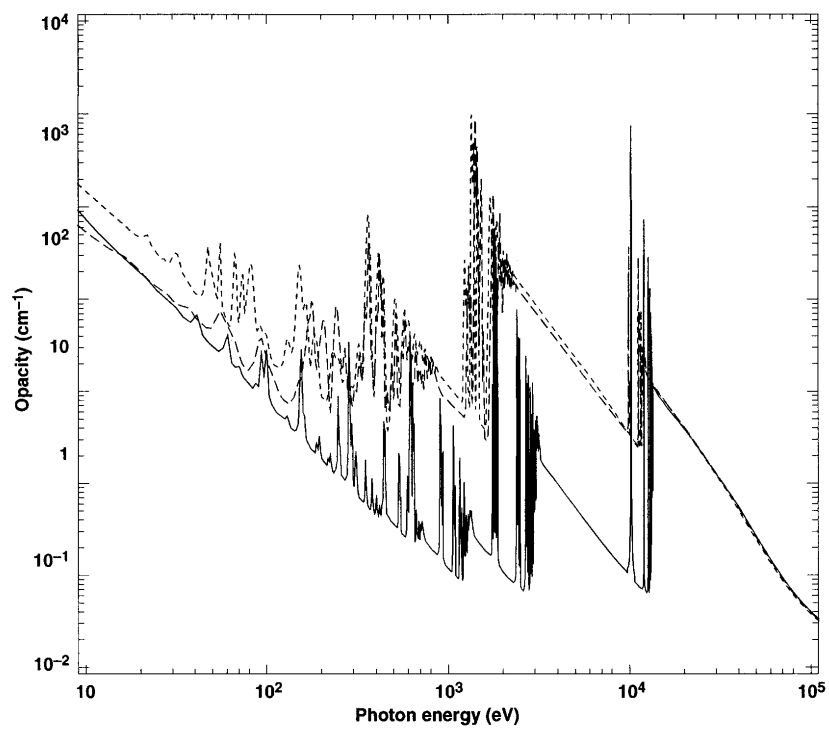
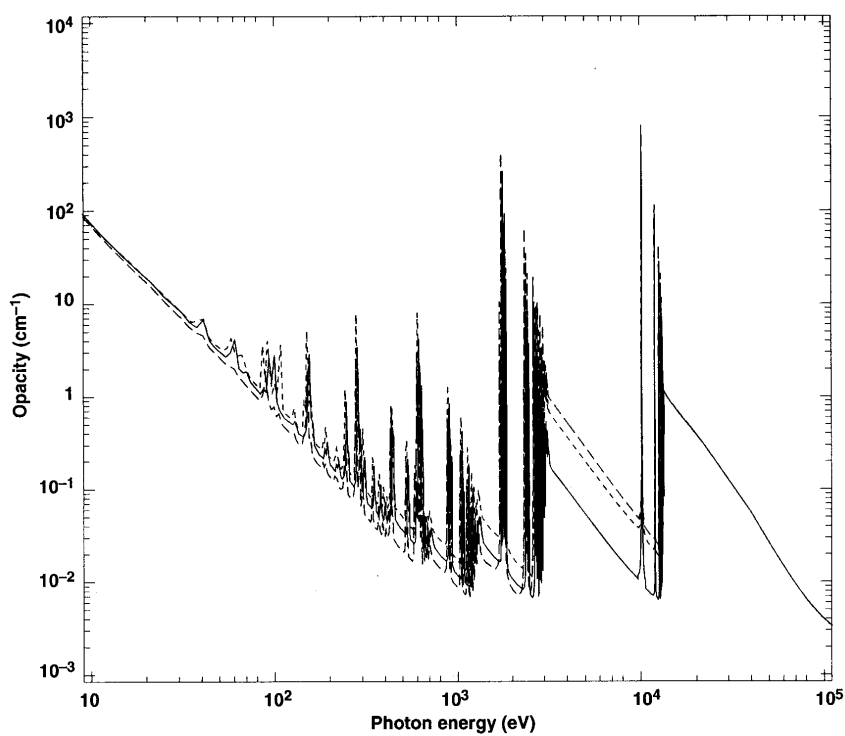


FIG. 8. Calculated opacities in cm^{-1} of germanium at $kT = 0.5$ keV and at 0.01 g/cm^3 density with $x_R = 0$. Full curve: LTE; long-dashed curve: full non-LTE based on the rate equations; short-dashed curve: LTE with the equivalent LTE temperature of 0.11523 keV from Table I.

FIG. 9. Same as Fig. 8 with $x_R = 10^{-4}$.FIG. 10. Same as Fig. 8 with $x_R = 10^{-2}$.

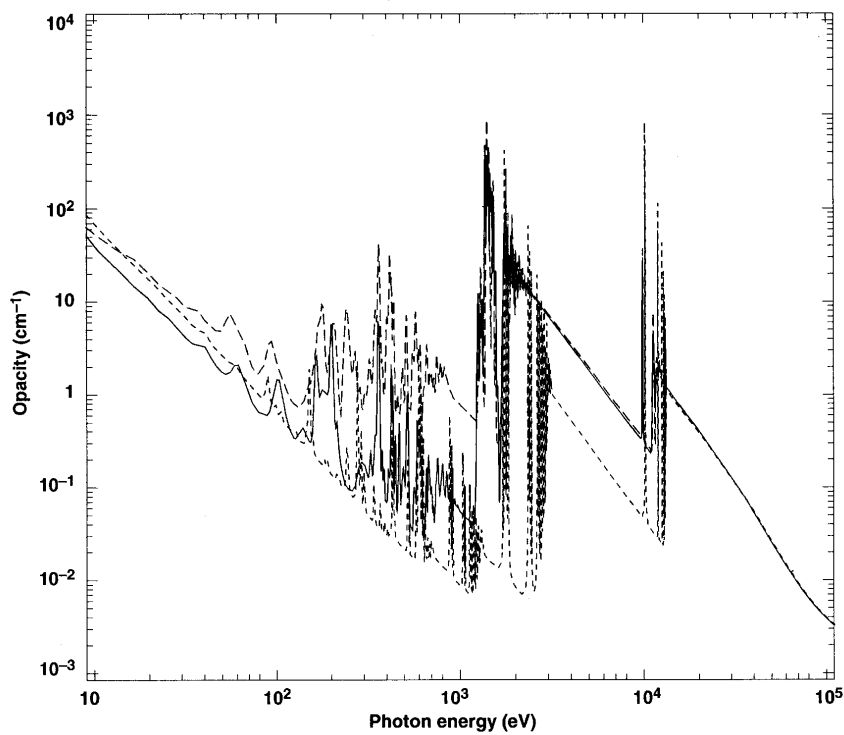


FIG. 11. Comparison of calculated opacities of germanium at $kT=0.5$ keV and at 0.01 g/cm³ density with different x_R with the prediction by LASNEX. Full curve: LASNEX; long-dashed curve: $x_R=10^{-4}$; short-dashed curve: $x_R=10^{-2}$.

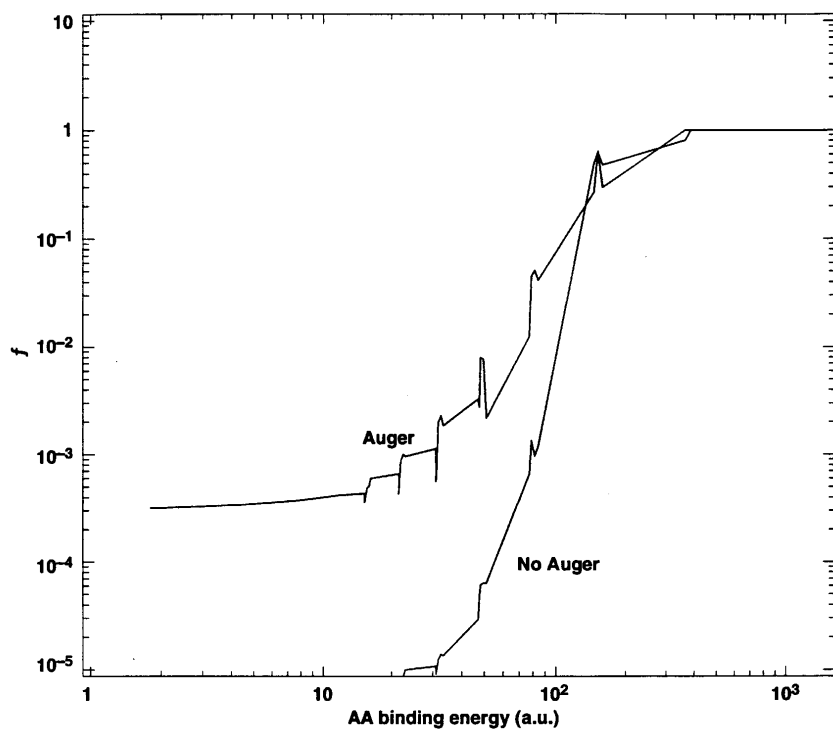


FIG. 12. Fermi functions of praseodymium at $kT=1$ keV and at 0.1 g/cm³ density with $x_R=10^{-4}$ with and without the Auger matrix elements in the rate equations.

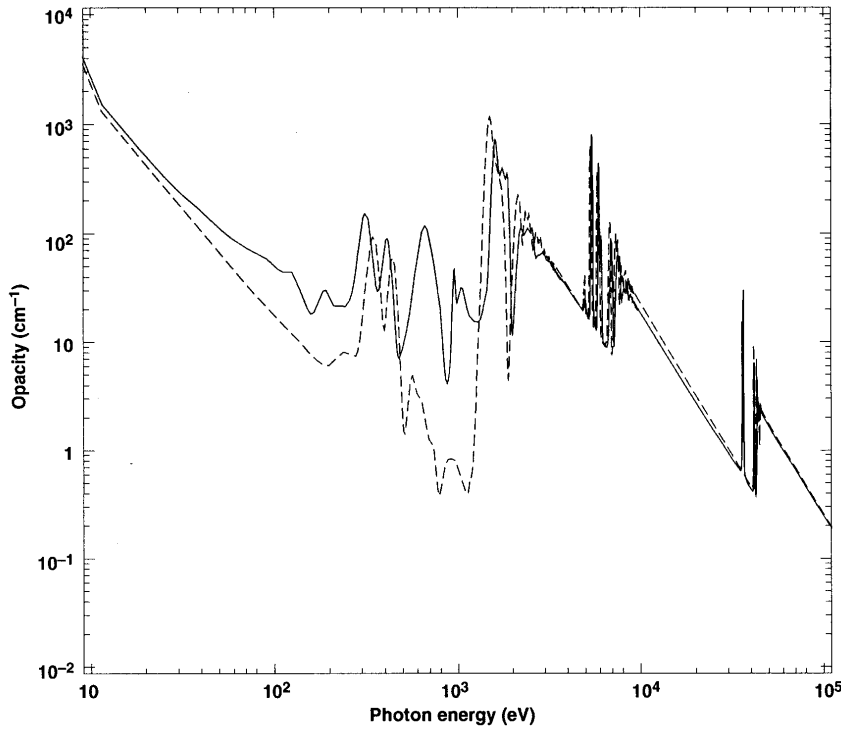


FIG. 13. Opacity of praseodymium at $kT = 1$ keV and at 0.1 g/cm^3 density with $x_R = 10^{-4}$, with and without the Auger matrix elements in the rate equations are indicated by full and dashed curves, respectively.

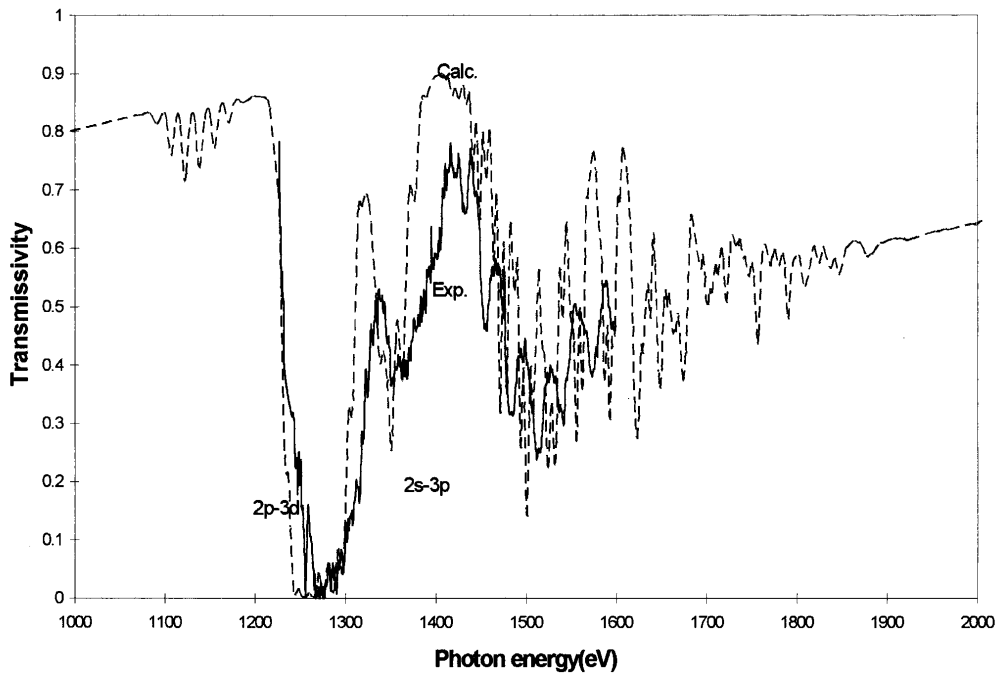


FIG. 14. Transmissivity of a germanium plasma of 3×10^{-3} -cm thickness at $kT = 76$ eV and $5 \times 10^{-2} \text{ g/cm}^3$ density. Experiment and calculation are given. The plasma is in LTE.

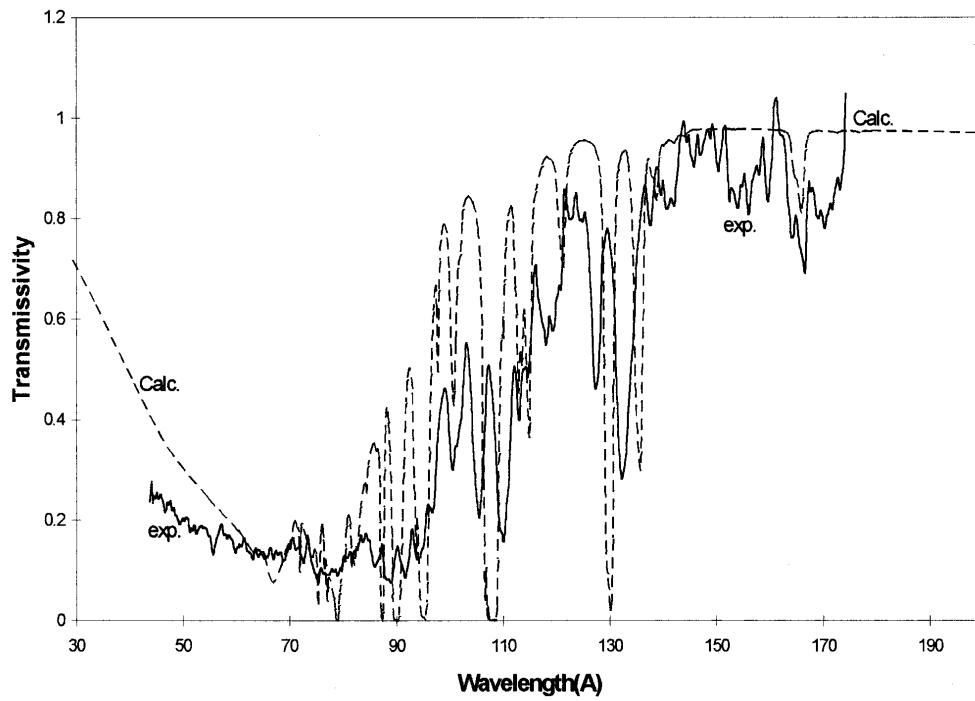


FIG. 15. Transmissivity of an aluminum plasma of 3×10^{-3} -cm thickness at $kT=20$ eV and 10^{-2} g/cm³ density. Experiment and calculation are given. The plasma is in LTE.

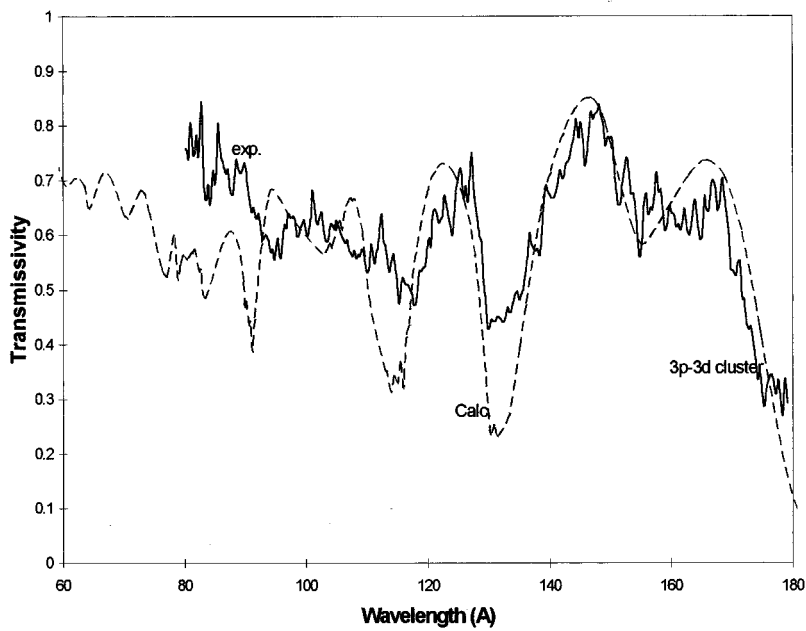


FIG. 16. Transmissivity of an iron plasma of 5×10^{-3} -cm thickness at $kT=22$ eV and 10^{-2} g/cm³ density. Experiment and calculation are given. The plasma is in LTE.

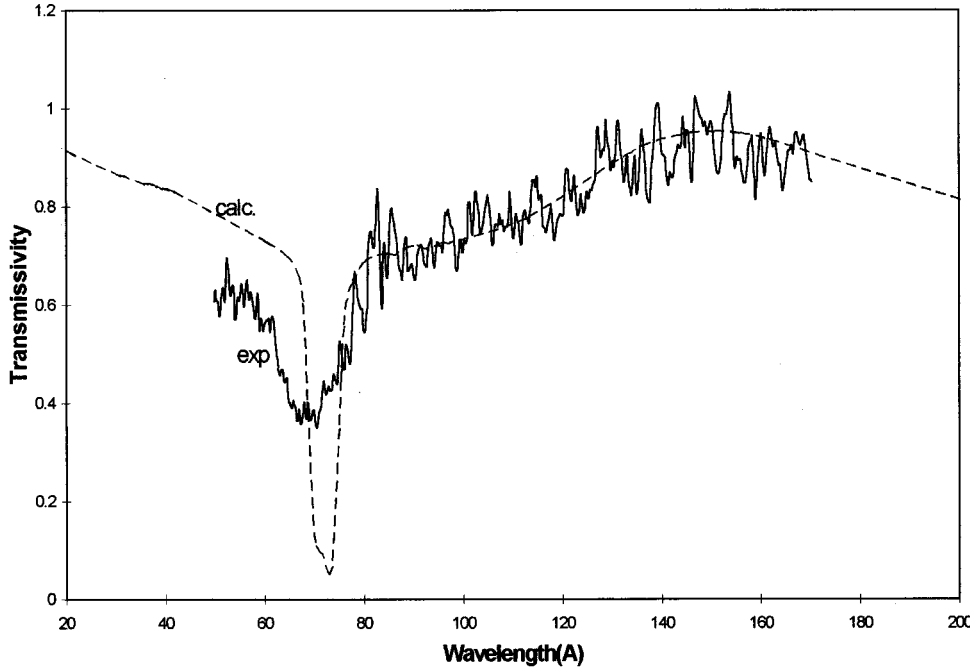


FIG. 17. Transmissivity of a holmium plasma of 5×10^{-4} -cm thickness at $kT = 20$ eV and 3.10^{-2} g/cm³ density. Experiment and calculation are given. The plasma is in LTE.

Equation (2.26) is generally valid for LTE or non-LTE ionization balance. Next, we take the approximation that the individual m terms in Eq. (2.26) are zero, which we will call the “one level in continuum” (OLC) approximation. The name is justified by observing that the OLC approximation is exact when there is only one bound level embedded in the continuum. The OLC approximation yields the following for the occupancy of the level m :

$$N_m = \frac{g_m \lambda_m}{\exp[(\mu - \epsilon_m)/kT] + \lambda_m}, \quad (2.27)$$

where

$$\lambda_m = \frac{R_{mc}^c N_c + R_{mc}^r + K_{cm}}{R_{mc}^c N_c + r_{mc}^r + K_{mc}}. \quad (2.28)$$

Equations (2.27) and (2.28) yield the Fermi statistics if $\lambda_m = 1$. That occurs if the plasma is optically thick in which case $P_c = 1$ and $r_{mc}^r = R_{mc}^r$ and in addition we must have $K_{cm} = K_{mc}$. In fact, using the detailed balance for the Auger transition rates, it is easy to show that as the level populations approach the LTE populations the last condition is satisfied. Also, in the limit when the background radiation field is negligible, r_{mc}^r is zero and R_{mc}^r is responsible for the radiative recombination and Eq. (2.28) leads to the corona equilibrium. The number of free electrons per AA, N_c , is obviously equal to Z minus the number of bound electrons. The individual occupancies of the bound levels given by Eqs. (2.27) and (2.28) are not exact because they are not the solutions of Eq. (2.23). However, their sum satisfies Eq. (2.26), therefore we adopt it as a reasonable approximation for the ionization state. This facilitates the iteration procedure of solving Eq. (2.23) by determining N_c from Eqs. (2.27) and (2.28) first and solving Eq. (2.23) for the bound state populations subsequently. In fact, the self-consistent solutions of Eqs. (2.23), (2.27), and (2.28) together with Eq.

(2.11) for the photon escape probability involve a hierarchy of iterations that we outline in the next section.

III. COMPUTATIONAL RESULTS

The rate equations (2.23) and (2.24) in terms of the bound level occupancies and N_c are cubic, which necessitates the application of iteration schemes for the solution. In addition, all solutions must be also self-consistent with the frequency-dependent photon escape probability. In order to make the whole problem computationally tractable we adopted the following iteration scheme: (1) We start from the self-consistent LTE problem as described in Refs. [6] and [8] and compute all the rate constants from the LTE wave functions and from the LTE photon escape probability. (2) Next we obtain the first iteration value for N_c in the OLC approximation using Eqs. (2.27) and (2.28). (3) Next we solve Eq. (2.23) for the bound level populations by successive iterations where the availability factors a_m and $(g_m - N_m)$ for the n -th iteration are taken from the $(n-1)$ th iteration we iterate until the values of N_m converge. At this point the AA problem is solved in the first iteration. (4) In order to obtain realistic photoabsorption cross sections and photon escape probabilities one must go beyond the AA model and build into the model the effect of “detailed configuration accounting” (DCA) due to the many-electron configurations. This necessitates calculating the statistical distribution of the numerous DCA states, which in a system not in LTE is a serious problem in itself. We solve this problem by calculating an “equivalent LTE temperature” kT_{eq} , which after Busquet [22] is defined as the temperature that, under LTE condition, yields the same value for N_c as the non-LTE problem. We also calculate an equivalent Fermi level μ_{eq} , which together with kT_{eq} is used to calculate an equivalent Boltzmann distribution of the many-electron DCA states. We proceed to compute the photoabsorption from these DCA states as described in Ref. [8]. (5) Having obtained the non-LTE

photoabsorption cross section and non-LTE populations in this manner in the first iteration we go back to point (1) and iterate until convergency is reached. In the calculations presented here convergency was reached usually after 4 or 5 iterations.

All the above iterations make the calculations rather lengthy compared to the LTE problems. We present two sets of calculations in which we investigate the effect of optical thickness, one for praseodymium ($Z=59$) at $kT=1$ keV and at 0.1 g/cm³ density and one for germanium ($Z=32$) at $kT=0.5$ keV and at 0.01 g/cm³ density. Calculations for the first case for an optically thin plasma and using the method of “equivalent LTE temperature” were published in Ref. [22], the second was a study case at a conference [9] where the author presented non-LTE corona equilibrium opacities obtained from level populations predicted by the LASNEX code of the Lawrence Livermore National Laboratory. The calculations for various optical thickness show that the results converge, as expected, to the LTE case when the plasma gradually becomes optically thick. We label the parameter for characterizing the optical thickness by x_R , which is the distance of the central ion from the edge of the semi-infinite slab divided by the LTE Rosseland mean length L_R .

The conditions for praseodymium at 1 keV and for germanium at 0.5 keV are summarized in Table I where we give the parameters x_R in column 1, the equivalent LTE temperatures in column 2, the numbers of free electrons per AA in column 3, and the degeneracy parameters of the free electron gas μ/kT and $\mu_{\text{eq}}/kT_{\text{eq}}$ in columns 4 and 5, respectively. The calculations for praseodymium are shown in Figs. 1–7, and also in Figs. 12 and 13. Figure 1 shows the self-consistent photon confinement factors P_c for three cases of x_R . Figure 2 shows the Fermi functions, defined as N_m/g_m versus the binding energies (in atomic units) of the self-consistent AA levels for four cases of optical thickness together with the LTE case. We can see that curve IV, corresponding to the case when the radiating ion is one Rosseland mean length away from the edge of the slab, practically coincides with the LTE curve, even when the photon confinement factors are not 1 for all photon energies. Figures 3 and 4 compare the LTE Fermi functions with those calculated in the OLC approximation and with the full non-LTE rate equations. It should be noted that strictly speaking Figs. 2–4 should be discrete, but for low binding energies the levels are closely spaced and they form a quasi-continuous distribution. In Figs. 2–4 the spikes in the non-LTE Fermi functions reflect the fact that adjacent levels with different angular momentum quantum numbers sometimes are populated very unevenly. The calculated opacities for praseodymium are shown on Figs. 5, 6, and 7 for $x_R=0$, 10^{-4} , and 10^{-2} , respectively. In each figure we compare the LTE opacities with that of the full non-LTE calculations and also with the LTE calculations using the equivalent temperatures of Table I. For the non-LTE calculations the distribution of the DCA states is computed with the aid of the equivalent LTE temperatures and Fermi level. The number of DCA states that contribute significantly to the opacities can be quite numerous, for example, the opacity in Fig. 6 was obtained using 144 DCA configurations distributed over 12 different degrees of ionization. It is out of the scope of this paper to discuss further

details of the DCA states and such details of the opacity calculations as line profiles, bremsstrahlung, and photoionization. For those the reader is referred to Refs. [4], [6], [8], and [15] and references quoted there. Here we concentrate only on the non-LTE AA level populations. For praseodymium in all cases the K shell is completely full and the L -shell populations do not differ much. Big differences occur for the M shell and higher shells. This is reflected in Figs. 5–7 where the opacities for photon energies above the L -shell lines and edges are close. For low photon energies the opacity is dominated by inverse bremsstrahlung, which differs due to the different degrees of ionization. Also, for the equivalent temperature LTE calculations the inverse bremsstrahlung is calculated by using the equivalent LTE temperature for the free electrons. The calculated opacities for the germanium at 0.5 keV are shown in Figs. 8, 9, 10, and 11. Figures 8, 9, and 10 are analogous to those of Figs. 5, 6, and 7. However, in the case of germanium the differences between the LTE and non-LTE populations occur already in the L shell, so the LTE and non-LTE opacities are close only beyond the K -shell edge. In Fig. 11 we compare the non-LTE opacities with $x_R=10^{-4}$ and 10^{-2} with that of an earlier calculation where the non-LTE AA populations were obtained by the radiation transport code LASNEX. Therefore, the solid curve in Fig. 11 represents a calculation where the non-LTE populations are not self-consistent within the model but were so to speak “borrowed” from another code. Since the LASNEX code uses a somewhat simple atomic physics package, the apparent differences are not surprising. It is interesting to note though that the LASNEX curve is close to the self-consistent non-LTE curve with $x_R=10^{-4}$ for photon energies beyond the L -shell threshold to that with $x_R=10^{-2}$ below the L -shell threshold. We also note that the LASNEX populations were obtained for the optically thin case ($x_R=0$).

In Figs. 12 and 13 we show the effect of the presence or absence of the Auger matrix elements for one case of the praseodymium set. Figure 12 shows the Fermi functions for the AA levels. It is evident that in the absence of the Auger transitions the occupancies of the upper levels are depleted, thus considerably reducing the photoabsorption at photon energies below the M shell, as shown in Fig. 13.

Direct experimental verifications of non-LTE effects are not known to the author. Opacity experiments were published recently for germanium at $kT=76$ eV [23] and for aluminum, iron, and holmium in the $kT=20$ eV region [24]. The experimental data were published in terms of the transmissivity of a slab of certain thickness of the hot plasma. We investigated the possible non-LTE features of the above experiments by solving the steady-state rate equations and found that in each case the plasma was actually in LTE. The comparison of the calculated transmissivities with experiments are shown in Figs. 14–17. The calculated transmissivities were derived from the opacities. In view of the fact that the ratio of radiative to collisional transition rates is proportional to $(kT)^{1/2}/\rho$, it is not surprising that experiments below 100–200 eV show LTE conditions. We can expect non-LTE conditions at high-temperature, small-size plasmas, such as occur in laser compressed pellets.

IV. DISCUSSION

The purpose of this paper was to present a somewhat rudimentary model for estimating the non-LTE effects on photoabsorption in laboratory plasmas. For the radiation field around the plasma we used the Planckian field thinned out by the photon escape probability. Generalization of the model allowing any radiation field as an input is simple. Although experiments have been perfected to measure quantitatively LTE opacities of hot plasmas, up to about 100-eV plasma

temperature, the author is not aware of experiments that have concentrated on quantitative measurements of non-LTE effects. Since non-LTE effects are easier to detect at higher temperatures, as more powerful lasers become available, those experiments will be possible.

ACKNOWLEDGMENT

This work was performed under the auspices of the U.S. Department of Energy by Lawrence Livermore National Laboratory under Contract No. W-7405-Eng-48.

-
- [1] A. S. Edington, *The Internal Constitution of Stars* (Cambridge University Press, Cambridge, 1926).
- [2] R. P. Feynman, N. Metropolis, and E. Teller, *Phys. Rev.* **75**, 1561 (1949).
- [3] R. D. Cowan and J. Ashkin, *Phys. Rev.* **105**, 144 (1957).
- [4] T. R. Carson, D. F. Mayers, and D. W. Stibbs, *Mon. Not. R. Astron. Soc.* **140**, 483 (1968).
- [5] J. W. Zink, *Phys. Rev.* **176**, 279 (1968).
- [6] B. F. Rozsnyai, *Phys. Rev. A* **5**, 1137 (1972).
- [7] B. H. Armstrong and R. W. Nicholls *Emission, Absorption and Transfer of Radiation in Heated Atmospheres* (Pergamon, New York, 1972).
- [8] A. Goldberg, B. F. Rozsnyai, and P. Thompson, *Phys. Rev. A* **34**, 421 (1986).
- [9] For a comprehensive report on hot plasma opacities, see *Proceedings on the "Third International Opacity Workshop, WorkOp-III:94,"* edited by A. Rickert, K. Eidmann, J. Meyer-Ter-Vehn, F. J. D. Serduke, and C. A. Iglesias (Max-Planck Institut fur Quantenoptik, Garching, Germany, 1995).
- [10] D. R. Bates, F.R.S., A. E. Kingston, and R. W. P. McWhirther, *Proc. R. Soc. London, Ser. A* **270**, 297 (1962).
- [11] Y. T. Lee, G. B. Zimmerman, D. S. Bailey, D. Dickson, and D. Kim, in *Radiative Properties of Hot Dense Matter III*, edited by B. Rozsnyai, C. Hooper, R. Cauble, R. Lee, and J. Davis (World Scientific, Singapore, 1987).
- [12] D. Duston and J. Davis, *Phys. Rev. A* **21**, 1664 (1980).
- [13] D. Duston and J. Davis, *Phys. Rev. A* **23**, 2602 (1981).
- [14] J. P. Apruzese, J. Davis, D. Duston, and K. G. Whitney, *J. Quant. Spectrosc. Radiat. Transf.* **25**, 479 (1981).
- [15] Y. T. Lee, *J. Quant. Spectrosc. Radiat. Trans.* **38**, 131 (1986).
- [16] B. F. Rozsnyai, *J. Quant. Spectrosc. Radiat. Transf.* **17**, 77 (1977).
- [17] W. Lotz, *Astrophys. J. Suppl.* **XIV**, 207 (1967).
- [18] B. F. Rozsnyai, V. L. Jacobs, and J. Davis, *Phys. Rev. A* **21**, 1798 (1980).
- [19] F. E. Irons, *J. Quant. Spectrosc. Radiat. Transf.* **22**, 1 (1979); **22**, 21 (1979); **22**, 37 (1979).
- [20] J. C. Weisheit, *J. Quant. Spectrosc. Radiat. Transf.* **22**, 585 (1979).
- [21] Y. T. Lee, R. A. London, and G. B. Zimmerman, *Phys. Fluids B* **2**, 2731 (1990).
- [22] M. Busquet, *Phys. Fluids B* **5**, 4191 (1993).
- [23] J. M. Foster *et al.*, *Phys. Rev. Lett.* **67**, 3255 (1991).
- [24] G. Winhart *et al.*, *J. Quant. Spectrosc. Radiat. Transf.* **54**, 437 (1995).